Published in final edited form as:
Cell Metab. 2012 November 7; 16(5): 672–683. doi:10.1016/j.cmet.2012.10.004.

A quantitative map of the liver mitochondrial phosphoproteome reveals post-translational control of ketogenesis

Paul A. Grimsrud[1,2,6], **Joshua J. Carson**[1,6], **Alex S. Hebert**[2,5], **Shane L. Hubler**[2,5], **Natalie M. Niemi**[1], **Derek J. Bailey**[2,5], **Adam Jochem**[1], **Donald S. Stapleton**[1], **Mark P. Keller**[1], **Michael S. Westphall**[5], **Brian S. Yandell**[3], **Alan D. Attie**[1], **Joshua J. Coon**[2,4,5], and **David J. Pagliarini**[1,*]

[1]Department of Biochemistry, University of Wisconsin – Madison, Madison, WI 53706

[2]Department of Chemistry, University of Wisconsin – Madison, Madison, WI 53706

[3]Department of Statistics, University of Wisconsin – Madison, Madison, WI 53706

[4]Department of Biomolecular Chemistry, University of Wisconsin – Madison, Madison, WI 53706

[5]Genome Center of Wisconsin

Summary

Mitochondria are dynamic organelles that play a central role in a diverse array of metabolic processes. Elucidating mitochondrial adaptations to changing metabolic demands and the pathogenic alterations that underlie metabolic disorders represent principal challenges in cell biology. Here, we performed multiplexed quantitative mass spectrometry-based proteomics to chart the remodeling of the mouse liver mitochondrial proteome and phosphoproteome during both acute and chronic physiological transformations in more than 50 mice. Our analyses reveal that reversible phosphorylation is widespread in mitochondria, and is a key mechanism for regulating ketogenesis during the onset of obesity and type 2 diabetes. Specifically, we have demonstrated that phosphorylation of a conserved serine on Hmgcs2 (S456) significantly enhances its catalytic activity in response to increased ketogenic demand. Collectively, our work describes the plasticity of this organelle at high resolution and provides a framework for investigating the roles of proteome restructuring and reversible phosphorylation in mitochondrial adaptation.

Introduction

Mitochondria are key centers of metabolism and signaling for nearly all eukaryotic cells (Nunnari and Suomalainen, 2012). Mitochondrial dysfunction is associated with a spectrum of rare inborn errors of metabolism and an increasing number of common diseases including Parkinson's, Alzheimer's, various cancers and type 2 diabetes (T2D) (Nunnari and Suomalainen, 2012; Szendroedi et al., 2012). Recent large-scale efforts have helped to define the mammalian mitochondrial proteome and to reveal its variability across tissues (Foster et al., 2006; Johnson et al., 2007; Pagliarini et al., 2008). Collectively, this work has advanced our understanding of basic mitochondrial biology and has catalyzed the discovery

*Correspondence: pagliarini@wisc.edu.
[6]These authors contributed equally to this work

of gene mutations underlying many mitochondrial diseases (Calvo and Mootha, 2010). Nonetheless, important steps remain for achieving a systems-level understanding of this organelle and its contribution to disease pathophysiology. These include elucidating the proteome remodeling that accompanies conditions involving mitochondrial dysfunction and, more comprehensively, defining the role of post-translational modifications (PTMs) in regulating mitochondrial protein activities.

Mounting evidence suggests that mitochondrial adaptation relies on a range of reversible PTMs. Already, focused efforts have linked the importance of these modifications to apoptosis, oxidative phosphorylation, the hypoxia response, and mitochondrial biogenesis (O'Rourke et al., 2011; Pagliarini and Dixon, 2006), and large-scale studies have revealed that much of the mitochondrial proteome is phosphorylated (Boja et al., 2009; Deng et al., 2010; Zhao et al., 2011) or acetylated (Guan and Xiong, 2011). Nevertheless, our understanding of specific protein and PTM alterations that affect mitochondrial function remains in its infancy. This is principally due to the fact that large-scale investigations of PTMs often fail either to identify the specific sites of modification or to quantify how these modifications (and the abundances of the modified proteins) change in a condition-specific manner.

Here, we performed multiplexed quantitative proteomics and site-specific phosphoproteomics of mouse liver mitochondria across a series of contrasting biological states (Figure 1A, 4A). We analyzed lean (wild type) and obese (leptin deficient) mice at two ages (4 weeks or 10 weeks), each from two strains (C57BL/6J (B6) and BTBR). These analyses were primarily motivated by the suspected contribution of mitochondrial dysfunction to the onset of obesity and insulin resistance (Szendroedi et al., 2012), and by the sharp contrast in T2D susceptibility between these two strains (Keller et al., 2008). To achieve extensive coverage, and to quantify fold-changes between conditions, we conducted five independent 8-way comparisons (40 mice total, Figure 1A) using high resolution and high mass accuracy mass spectrometry (MS) with isobaric tagging (Lee et al., 2011; Phanstiel et al., 2011; Ross et al., 2004; Thompson et al., 2003). Using this same approach, we also assessed the reversibility of these modifications in wild type B6 mice during acute fasting and refeeding (Figure 4A). Collectively, we identified 811 phosphosites—including more than 100 not previously reported—on 295 mitochondrial proteins, and have revealed that a large proportion of these modifications are dynamic and reversible during these acute and chronic transformations.

We leveraged this quantitative dataset to reveal that phosphorylation is an important mechanism for regulating ketone body production. We have demonstrated that Hmgcs2, which catalyzes the first committed step of ketogenesis (Reed et al., 1975), is phosphorylated on 10 separate residues. Phosphorylation of five of these sites change dynamically across our biological conditions ($q<0.1$), and at least one—phosphorylation of serine 456—significantly enhances enzyme activity. We have further shown that phosphorylation of this site occurs in response to increased ketogenic demand both in cell culture and in our mouse models, whose serum β-hydroxybutyrate increase with obesity and the onset of T2D. Our protein and phosphorylation compendium, termed MitoMod, is freely available at: mitomod.biochem.wisc.edu.

Results and Discussion

Comparative Proteomic Analyses of Mouse Liver Mitochondria

The goal of our initial proteomic analyses was to establish a comprehensive and quantitative map of mitochondrial protein abundance and site-specific protein phosphorylation levels across the contrasting biological conditions of age, mouse strain, and obesity status. To do

so, we performed these analyses in two phases. In the *univariate* phase, we analyzed liver mitochondria from four lean (wild type) and four obese (leptin$^{-/-}$, *ob/ob*) 10 week-old B6 mice (Figure 1A). This initial phase enabled us to assess the breadth and depth at which our analysis platform could detect changes to the mitochondrial proteome and phosphoproteome. In the *multivariate* phase, we analyzed 40 mice differing by three variables: age, strain, and obesity (Figure 1A). These animals included lean (wild type) and obese (*ob/ob*) mice from both diabetes-susceptible (BTBR) and diabetes-resistant (B6) strains, each as either adolescents (4 weeks of age) or adults (10 weeks of age).

For each phase, we purified mitochondria only to the extent required to achieve near comprehensive coverage of the liver MitoCarta protein list, allowing us to simultaneously profile co-purifying organelles (MitoCarta is a tissue-specific compendium of mitochondrial proteins complied using mass spectrometry-based proteomic analyses of highly purified mitochondria, machine learning, and GFP microscopy (Pagliarini et al., 2008)). Our univariate phase identified 3,447 unique proteins and 3,895 unique phosphoisoforms (site-specific phosphorylation patterns) from just over 1 million MS/MS scans. These include 692 of the 700 liver MitoCarta proteins, and 449 mitochondrial phosphoisoforms. Notably, unsupervised hierarchical clustering of the protein abundance measurements appropriately grouped the mice by their obesity status (Figure 1B). After correcting for multiple hypotheses, significant differences ($q<0.1$) in abundance were observed for 1,014 proteins (325 mitochondrial, Figures 1H and S1B) and 720 phosphoisoforms (102 mitochondrial, Figure 1H and S1D).

Our univariate data revealed extensive and reproducible remodeling of the liver mitochondrial proteome and phosphoproteome with obesity (Figure 1B-D, S1B-D). For example, fatty acid oxidation and oxidative phosphorylation (OxPhos) proteins were increased with obesity (Figure 1C,G), while reactive oxygen species (ROS) detoxification enzymes were decreased (Figure S1C), consistent with known liver alterations (Buchner et al., 2011; Deng et al., 2010; Wang et al., 2012a). Phosphorylation changes were also prominent in a range of central mitochondrial (and non-mitochondrial) pathways (see mitomod.biochem.wisc.edu and Tables S1-5). For example, the three most statistically significant changes ($q<0.002$) in phosphorylation of MitoCarta proteins in this phase were found on enzymes involved in ketogenesis (Hmgcs2), lipogenesis (Gpam), and retinol metabolism (Dhrs4)—pathways key for proper liver function and linked to changes caused by obesity (Bonet et al., 2012; Szendroedi et al., 2012).

Given the efficacy of our univariate phase, we proceeded to analyze 40 additional mice in our multivariate phase (Figure 1A). This experiment enabled us to identify changes linked to specific variables including age, obesity status, mouse strain, and combinations thereof (see Figure S1A for a description of all possible comparisons). Here, we identified 3,684 unique proteins, including 98% of the liver mitochondrial proteins previously identified by MS in the MitoCarta study (Pagliarini et al., 2008). Of the 5,948 unique phosphoisoforms identified, 508 are on mitochondrial proteins. Interestingly, hierarchical clustering of MitoCarta protein abundances grouped these mice primarily by strain, with secondary groupings of either obesity status (B6) or diabetic status (BTBR) (Figure 1F). Our data also reveal that the diabetic 10 week-old BTBR mice, opposite their B6 counterparts, have repressed expression of glycolytic and TCA cycle enzymes (Figure S1G, Table S6), consistent with a ketogenic state (Berry et al., 1983). Similarly, while OxPhos proteins are induced with obesity in B6 mice, they are decreased in obese hyperglycemic BTBR mice (Figure 1G, Table S6), perhaps partially explaining discrepancies in the effects of obesity on liver mitochondrial respiration in different mouse models (Buchner et al., 2011; Holmstrom et al., 2012).

Across all conditions assessed in these two phases, we have identified significant changes ($q<0.1$) in 268 mitochondrial phosphoisoforms on 136 proteins, and abundance alterations for 534 mitochondrial proteins. Importantly, our separate analyses also demonstrate that our measurements are both accurate and reproducible (Figures 1B-E, Figure S1B-F). Together, these analyses begin to capture the global plasticity of the mitochondrial proteome, and highlight individual proteins and pathways in this organelle that are key to cellular metabolic adaptation during various physiological transformations (Figure 1H, Tables S1-5).

A Quantitative Map of Mitochondrial Phosphoproteome Dynamics

The results of our univariate and multivariate experiments expand the number of known mouse liver mitochondrial phosphosites by 123 (including many on proteins of low abundance, Figure S2), while capturing 77% of those reported previously (Huttlin et al., 2010; Lee et al., 2007; Monetti et al., 2011; Villen et al., 2007). Our analyses also help to discern which proteins might be particularly important targets of phosphorylation in several ways. First, by organizing the mitochondrial proteome into pathways and complexes (Figure 2), it is clear that certain proteins have a disproportionately high number of phosphorylation sites, even when the corresponding proteins are each detected at comparable levels. Such proteins include Atp5a1 of the OxPhos machinery (Figure 2A) and Hmgcs2 of the ketogenesis pathway (Figure 2B), which each have at least three-fold more phosphorylation sites than other members of their respective pathways. Second, by comparing our data with a recent muscle phosphoproteomic study (Zhao et al., 2011), we find a high degree of overlap in phosphorylation targets for certain pathways (*e.g.* 15 of our 27 phosphorylated OxPhos subunits, Figure 2A), suggesting that a common set of proteins are subject to phosphorylation in different tissues. Third, because our approach quantifies phosphorylation levels across a range of conditions, we can identify sites that are modified dynamically. We find that a large proportion (41%) of mitochondrial phosphorylation levels significantly and reproducibly change ($q<0.1$) between at least one of our comparison groups (Figure S1A). As illustrated in Figure 2A, residues on 14 of the 27 phosphorylated OxPhos subunits noted above are subject to dynamic phosphorylation ($q<0.1$), and thus represent likely regulatory sites (red dots in Figure 2A).

The design of our multivariate study enables us to associate specific protein and phosphorylation changes with particular physiological transitions. Of the 235 mitochondrial phosphoisoforms that significantly change in our multivariate dataset ($q<0.1$), 134 demonstrate associations with age, mouse strain, or onset of obesity, independent of other factors (Figure 3A, Table S3). For example, phosphorylation of serine 162 on Lactb increases specifically in an age-dependent manner in both strains, regardless of their obesity status (Figure 3B). The increased phosphorylation of Lactb on S162 in 10 week-old mice could potentially contribute to the development of obesity in adult mice, as the Lactb gene has been causally linked with this condition (Chen et al., 2008). Likewise, the phosphorylation levels of serine 55 on Acadl and threonine 46 on Slc25a5 were significantly altered in strain- and obesity-centric manners, respectively (Figure 3B). Acadl catalyzes the first step in mitochondrial beta-oxidation of long straight-chain fatty acids (Lea et al., 2000). We hypothesize that the increase in phosphorylation of S55 on Acadl in BTBR mice promotes enhanced lipid oxidation, consistent with their resistance to the development of fatty liver (Wang et al., 2012a). Collectively, these examples of condition-specific changes in mitochondrial phosphorylation reveal how our data can be leveraged to generate hypotheses about how a given site affects protein function and to elucidate important mitochondrial processes that are altered in defined physiological states.

Acute Mitochondrial Phosphorylation Changes During Fasting/Refeeding

Our multivariate analyses described above provide a map of the liver mitochondrial phosphoproteome, and describe how individual phosphosites are altered during gradual, long-term physiological changes. Next, to ensure that many of the phosphorylation events we detect represent reversible sites of modification, and to further refine our hypotheses about the function of individual phosphosites, we measured changes in the mitochondrial phosphoproteome during an acute fasting/refeeding experiment. Here, eight lean (wild type) B6 mice were fasted overnight (16 hrs), after which half of the animals were allowed to feed *ad libitum* for two hours (Figure 4A). Serum metabolite analyses revealed the expected refeeding responses: insulin and glucose levels were elevated and β- hydroxybutyrate and triglyceride levels were diminished in refed versus fasted animals (Figure 4B).

Refeeding caused rapid changes to 88 MitoCarta phosphoisoforms (58 decreasing and 30 increasing at $q<0.1$), with generally small or nonexistent underlying changes to protein levels (Figure 4D). Notably, these included expected decreases (Pagliarini and Dixon, 2006) in the phosphorylation of pyruvate dehydrogenase E1α S232, S293 and S300 and branched chain ketoacid dehydrogenase E1 S338 (Figure 4C). Likewise, expected changes to non-mitochondrial proteins were observed, including increased phosphorylation of glycogen synthase kinase 3 alpha S21 (Fang et al., 2000) and decreased phosphorylation of inositol 1,4,5-triphosphate receptor 1 S1588 (Wang et al., 2012b) (Figure 4C). We again observe dynamic phosphorylation on mitochondrial proteins from a wide range of processes, including oxidative phosphorylation (Atp5a1, Atp5j, Ndufv3, Cox4i1), the TCA cycle (Idh3g), fatty acid oxidation (Acaa1b, Acadvl, Hadha, Ehhadh), the urea cycle (Glud1, Slc25a13, Otc, Cps1), hormone metabolism (Comt), and glycerolipid biosynthesis (Gpam). These dynamic phosphorylation events could contribute to known changes to these pathways in fasting, aging, and the onset of obesity (Nunnari and Suomalainen, 2012; Szendroedi et al., 2012). These data also suggest that proteins involved in heme biosynthesis (Alas1), synthesis of mitochondrial-specific fatty acids (Mcat), and protein translation (Rg9mtd1, Mrpl1, Mrpl45, Mrps36), among others, are subject to rapid, post-translational regulation in response to refeeding (Figure 4D, Table S7). Collectively, this analysis demonstrates that mitochondrial protein phosphorylation is reversible and responsive to acute metabolic perturbations.

Kinase Activities Predicted *via* Phosphopeptide Data

Our observation that dynamic phosphorylation is widespread among mitochondrial proteins motivated us to investigate which kinases might be performing these modifications. To do so, we employed two phosphosite analyses. First, we directly searched our data for phosphorylation within known kinase motifs, as defined in the PHOSIDA database (Gnad et al., 2011). This analysis suggested that a wide variety of kinases might be active in this organelle: 13 different kinases were each associated with at least 20 MitoCarta phosphosites (Figure 5A). This analysis, however, does not take into account the frequency at which each sequence appears in the proteome and is biased toward established kinase motifs. Given these shortcomings, we also analyzed our data using the Motif-X algorithm (Schwartz and Gygi, 2005), which identifies amino acid residues overrepresented at specific positions around phosphorylation sites. Motif-X analysis revealed four such amino acid sequences around MitoCarta phosphosites, including those that loosely match to the CK2 (sxxE) and PKA (Rxxs) consensus motifs (Figure 5B). Together, these analyses suggest that PKA and CK2 are among the active kinases in mitochondria, consistent with recent phospho-motif analysis of muscle mitochondrial proteins (Zhao et al., 2011), and with reports of PKA phosphorylating complex IV subunits (Acin-Perez et al., 2009). Furthermore, across our entire multivariate dataset (mitochondrial and non-mitochondrial proteins), phosphorylation levels on proteins with putative PKA and CK2 motifs increase in an age- and obesity-

dependent manner ($p<0.05$), suggesting that these kinases may be responsible for some of the increased mitochondrial phosphorylation seen following these transitions (Figure 5C; see Figure S3 and Tables S1-5 for all motif and kinase activity predictions).

Phosphorylation of serine 456 on Hmgcs2 promotes ketogenesis

The combination of our quantitative phosphoproteomics data and kinase activity predictions enabled us to predict which phosphorylation events might regulate specific mitochondrial proteins. Among the most highly phosphorylated proteins in our study was Hmgcs2, the enzyme that catalyzes the rate-limiting step in ketogenesis (Reed et al., 1975). We identified 10 phosphorylated residues on Hmgcs2 (Figure 2B), and phosphorylation abundance on five of these sites exhibited significant changes in at least one comparison ($q<0.1$). Two of these sites, S433 and S456, are conserved in the human ortholog (HMGCS2) and had phosphorylation patterns that suggest a potential contribution to the elevated ketone body levels we observe in obese diabetic BTBR mice (Figure 6A), leading us to hypothesize that these phosphosites might regulate enzyme activity. Due to a primary sequence difference between B6 and BTBR mice near the S433 phosphorylation site (Figure S4A), we were unable to directly measure the relative abundance of this site between strains using the iTRAQ system. However, spectral counts suggest that phosphorylation of this site is only prominent in B6 animals (Figure S4A), where it exhibits an obesity-induced increase in 10 week-old mice ($q<0.03$). Alternately, S456 exhibits an obesity-induced increase in both strains, with a more pronounced increase in BTBR mice (Figures 6B,C). As highlighted in Figure 6D, S456 on Hmgcs2 falls within consensus motifs for both protein kinase A (PKA) and caseine kinase 2 (CK2)—two of the kinases predicted to be active in our mitochondrial survey (Figures 5, S3) and that have previously been associated with mitochondrial regulation (Acin-Perez et al., 2009; Schmidt et al., 2011; Zhao et al., 2011).

To evaluate the effects of these dynamic phosphorylation events on Hmgcs2 enzymatic activity, we performed biochemical assays on a series of human HMGCS2 variants. We mutated each phosphorylated residue to an acidic residue (aspartic acid or glutamic acid) to mimic phosphorylation (S433D, S456D/E) or to a non-phosphorylatable residue (alanine or methionine) to mimic dephosphorylation (S433A, S456A/M). We immunoprecipitated these mutants, along with wild type and catalytically inactive (C166A) HMGCS2, from HEK293 cells, and tested the activity of each variant in an *in vitro* enzymatic assay (Skaff and Miziorko, 2010). As seen in Figure 6E, the phosphomimetics for serine 456 each resulted in at least a 60% increase in enzyme activity over wild type and the S456A variant that was consistent across multiple substrate concentrations (Figure 6F) and protein amounts (Figure S4C). A third variant (S456M), which approximates the steric change of the phosphomimetics without conferring a negative charge, also had no increase in enzyme activity (Figure 6E). Interestingly, the S433 phosphomimetic had no change in activity (Figure 6E, S4B), suggesting that phosphorylation on this site has a role distinct from directly modifying Hmgcs2 enzymatic activity.

Given the kinase motifs surrounding S456 (Figure 6D), we tested the ability of PKA to activate enzyme activity by incubating it with wild type HMGCS2 and each of the S456 variants before repeating the activity assays. As seen in Figure 7A, only wild type HMGCS2, which possesses a phosphorylatable serine 456, had its activity increased by PKA. MS analysis of the PKA-treated HMGCS2 verified that serine 456 was indeed phosphorylated by this treatment (Figure 7B), and that the untreated enzyme had no detectible phosphorylation on this site. CK2 increased HMGCS2 activity to an even greater extent (Figure 7A) than PKA, with this effect likewise abrogated by mutation of S456. This result is consistent with the human ortholog of HMGCS2 (Figure 7B) having a slightly weaker PKA consensus site around S456 than the mouse ortholog (Figure 6B), while maintaining a strong CK2 consensus sequence.

We next sought to determine if S456 phosphorylation is important for the activation of HMGCS2 in response to increased ketogenic demand. To do so, we immunoprecipitated WT and mutant HMGCS2 from HEK293 cells cultured in either standard or ketogenic media, which increases ketone body production (Figure S5A) (Sengupta et al., 2010). WT HMGCS2 was approximately 2-fold more active when purified from cells grown in ketogenic media ($p<0.001$) (Figure 7C). This effect was ablated with mutation of S456 (Figure 7C), with neither the S456A or S456D mutants showing a change in activity between media conditions (note S456D activity was still greater than S456A activity, consistent with Figures 6E-F). Disruption of either the basic (K453A) or acidic (E458A) kinase motifs also abrogated HMGCS2 activity in ketogenic media (Figure 7D), although variants missing proline 457 behaved similarly to wild type (Figure S7D). Moreover, WT HMGCS2 purified from 293 cells grown in ketogenic media could not be further activated by *in vitro* phosphorylation with CK2, suggesting maximal phosphorylation occupancy of S456 in ketogenic conditions (Figure 7E).

As a final test of the importance of S456 phosphorylation on the activation of HMGCS2, we measured ketone body production from HEK293 cells expressing HMGCS2 variants. In standard media, 293 cells produce miniscule amounts of β-hydroxybutyrate (β-HB), in large part due to the nearly complete absence of HMGCS2 mRNA (Figure S5C). However, expression of exogenous HMGCS2 results in significant β-HB production, which is further activated by ketogenic media (Figure S5A) (Sengupta et al., 2010). Here, we expressed wild type, S456A or S456D HMGCS2 in 293 cells (Figure S5B) under both standard and ketogenic conditions and measured β-HB production after 72 hours. Consistent with our *in vitro* activity results (Figure 7C), mutation of S456 significantly attenuated the fold-change increase in ketone body production following a switch to ketogenic media (Figure 7F). Also consistently, cells harboring the 456D mutant had a greater ketogenic output than those with the S456A mutant (Figure 7G). Interestingly, cells expressing wild type HMGCS2 had the greatest total β-HB production. This suggests that, *in vivo*, mutation of this site might affect other properties of HMGCS2, such as proper mitochondrial localization, interactions with other proteins, or its modification by other known PTMs (*e.g.*, acetylation, succinylation, or palmitoylation) (Kostiuk et al., 2008; Quant et al., 1990; Shimazu et al., 2010). Nonetheless, the combination of our mass spectrometry analyses, *in vitro* enzyme activity measurements, and cellular ketone body assays strongly support a role for HMGCS2 S456 phosphorylation in enhancing ketogenic output.

Conclusion

We have established a quantitative proteomic compendium that charts dynamic changes in mitochondria across a series of contrasting biological states. This resource, termed MitoMod (mitomod.biochem.wisc.edu), captures both protein and phosphoprotein alterations, and is further leveraged by matched microarray data from the same tissue samples (Keller et al., 2008). These measurements enable the interrogation of post-transcriptional and post-translational mechanisms important for mitochondrial adaptation. Additionally, our quantitative data highlights mitochondrial alterations that track with distinct mouse strains and varying biological states, including the transition from adolescence to adulthood, the onset of obesity or T2D, and the response to acute fasting/refeeding. We demonstrate the utility of this resource by identifying Hmgcs2 S456 as an important phosphorylation target that enhances enzymatic activity in response to increased ketogenic demand.

While our work provides an in-depth assessment of mitochondrial phosphorylation, much remains to be learned about the nature and importance of this modification in regulating mitochondrial activities. Most notably, although our motif analyses have aided in identifying potential kinases responsible for the observed phosphorylation events, definitive demonstration of kinases residing within—or translocating to—mitochondria has largely

remained elusive (O'Rourke et al., 2011; Pagliarini and Dixon, 2006). As such, with few exceptions, we do not yet understand when, where, and how mitochondrial proteins are phosphorylated. Second, as PTMs are typically involved in rapid modulation of protein function, it will be important to continue to profile how the mitochondrial phosphorylation events we have identified change in response to other acute stresses, such as hypoxia, inflammation and elevated reactive oxygen species levels. Finally, because certain phosphorylation sites remain difficult to detect (including those within highly acidic peptides or those containing labile histidine phosphorylation) (Grimsrud et al., 2010b), it will be important to continue profiling the mitochondrial phosphoproteome with new MS technologies, such as negative electron-transfer dissociation (McAlister et al., 2012). Moving forward, we aim to address these issues, as well as to explore the interrelationship of phosphorylation with other prominent PTMs, including acetylation, methylation, and glycosylation. In doing so, we aim to elucidate the signaling networks that manipulate mitochondrial function, and to identify specific signaling molecules that can be targeted therapeutically to help remedy mitochondrial dysfunction in metabolic disease.

Experimental Procedures

Animal models

Breeding, sacrificing, and tissue harvesting of mice was described previously, for both the univariate (Zhao et al., 2009) and multivariate (Keller et al., 2008) experiments. Briefly, male mice were bred and housed in an environmentally controlled facility. Animals were provided access to water and standard rodent chow (Purina no. 5008), except during a fasting period (8 am–noon) in order to obtain plasma at 4 or 10 weeks of age, after which they were sacrificed by decapitation. Liver tissue was dissected, flash frozen with liquid N_2, and stored at −80°C until use. For the fasting/refeeding study, lean (wild type) B6 mice (9 weeks of age) were fasted overnight (16 hrs), after which half of the animals were allowed to feed *ad libitum* for two hours prior to sacrifice (note, fresh liver tissue was used for this experiment). All procedures were approved by the University of Wisconsin Animal Care and Use Committee.

Proteomics sample preparation

Tissue sections from each liver were used for mitochondrial enrichment, using previous methods (Pagliarini et al., 2008) modified by the addition of phosphatase inhibitors. Pelleted proteins (0.5 mg/sample) were digested as described (Grimsrud et al., 2010a), with modifications including sequential use of LysC and trypsin to ensure robust digestion. Peptides were labeled with a unique 8-plex iTRAQ reagent and samples were mixed in batches of eight. Peptides were separated by strong cation exchange chromatography (SCX), and after aliquots were removed for unmodified peptide quantitation, immobilized metal affinity chromatography (IMAC) was performed on each fraction to enrich for phosphopeptides as described (Phanstiel et al., 2011).

Large-scale tandem MS data collection and analysis

Nano-LC-MS/MS analysis was performed on an ETD-enabled LTQ Orbitrap Velos (Thermo Fisher Scientific). We performed data-dependent analysis with methods developed previously for improved quantitation accuracy with isobaric tags, relying on either post-acquisition filtering (PAF) (Phanstiel et al., 2011) or real-time filtering (RTF) (Wenger et al., 2011a) of precursors, for the univariate and multivariate experiments, respectively. Here, at least two runs using all HCD (Olsen et al., 2007) fragmentation were performed for each sample. An additional run using back-to-back ETD (Syka et al., 2004) and HCD on each precursor was performed on each phosphopeptide fraction. For the fasting/refeeding experiment, peptide and phosphopeptide fractions were subjected to two runs: one used all

HCD (applying PAF) and one used HCD along with our recently developed QuantMode method, which applies gas phase purification of precursors during data collection (Wenger et al., 2011a). We used our custom software COMPASS (Wenger et al., 2011b) to search the tandem MS data against a concatenated target-decoy UniProt mouse database, filter peptide identifications to 1% FDR, normalize iTRAQ reporter ion intensities, group peptides to parsimonious protein groups at 1% FDR, localize phosphorylation sites to specific residues at 95% probability, and sum reporter ion intensities for all spectra identifying the same protein or phosphoisoform in a given replicate.

Statistical analysis

Microsoft Access and Excel were utilized for statistical analysis of protein and phosphorylation measurements. We evaluated the significance of a given protein, phosphoisoform, or normalized phosphoisoform change by computing p-values, assuming a log-normal distribution for measurement error. Each comparison was made without adjustment for other factors or comparisons. We corrected for multiple hypothesis testing by computing a false discovery rate (FDR, q-value) where we assumed two populations (changing and unchanging) and that the unchanging population had p-values which are uniformly distributed from 0 to 1 (Figures S1E). FDR (q-values) were calculated separately for each measurement type. All protein and phosphoprotein measurements, as well as motif and kinase activity predictions are listed in Tables S1-5 (see Figure S1A for descriptions of all comparisons) and S7. Crosses (†) indicate significance at $q<0.1$ (applicable to all proteomic/phosphoproteomic measurements), with asterisks (*) indicating significance at $p<0.05$ (applicable to predictions in kinase/motif changes and biochemical assays).

MitoMod database development

All of the proteomic/phosphoproteomic data generated from this study were utilized to develop an interactive website, called MitoMod, that is freely available at mitomod.biochem.wisc.edu. The entire analyzed dataset, as well as the raw MS data (Thermo .raw files) and a table of all our iTRAQ tag-mouse pairings can also be downloaded for independent analysis.

Biochemical assessment of HMGCS2 regulation

HEK293 cells were cultured in DMEM supplemented with 10% FBS and antibiotics. All expression constructs were derived from pcDNA3.1 (Invitrogen) as described previously (Shimazu et al., 2010). Site-directed mutagenesis to create HMGCS2 variants was performed using standard PCR-based cloning techniques (constructs were verified by DNA sequencing). Transfections were performed at ~70% confluence and cells were lysed and protein subjected to immunoblotting with HRP-conjugated anti-FLAG antibody to assess expression. For ketogenic media (KM) experiments (Sengupta et al., 2010), cells were grown in KM (DMEM without the addition of FBS, and supplemented with 2mM sodium octanoate) from 24-72 hours after transfection, media collected at each time point, and ketone bodies measured using an Autokit Total Ketone Bodies assay (Wako). FLAG-tagged HMGCS2 was purified and its activity assessed as described previously (Shimazu et al., 2010; Skaff and Miziorko, 2010). See Supplemental Experimental Procedures for further details.

Supplementary Material

Refer to Web version on PubMed Central for supplementary material.

Acknowledgments

We thank Jonathan Stefely for help with Acetyl CoA synthesis, Alan Higbee and Xiao Guo for targeted MS analysis of HMGCS2 phosphorylation, Eric Verdin (UCSF) for generously donating HMGCS2 constructs, and John Denu and Kristin Dittenhafer for advice on the HMGCS2 activity assay. We also thank Danielle Swaney for advice on MS methodology, Douglas Phanstiel, Craig Wenger, and Nambirajan Rangarajan for informatics assistance, and AJ Bureta for assistance with figure illustrations. This work was supported by a Searle Scholars Award and by NIH grants RC1DK086410 (to D.J.P.), R01GM080148 (to J.J. Coon), R01DK058037 and R01DK66369 (to A.D.A.), F32DK091049 (to P.A.G.) and AHA grant 12PRE839 (to J.J. Carson).

References

Acin-Perez R, Salazar E, Kamenetsky M, Buck J, Levin LR, Manfredi G. Cyclic AMP produced inside mitochondria regulates oxidative phosphorylation. Cell metabolism. 2009; 9:265–276. [PubMed: 19254571]

Berry MN, Clark DG, Grivell AR, Wallace PG. The calorigenic nature of hepatic ketogenesis: an explanation for the stimulation of respiration induced by fatty acid substrates. Eur J Biochem. 1983; 131:205–214. [PubMed: 6832141]

Boja ES, Phillips D, French SA, Harris RA, Balaban RS. Quantitative Mitochondrial Phosphoproteomics Using iTRAQ on an LTQ-Orbitrap with High Energy Collision Dissociation. J Proteome Res. 2009; 8:4665–4675. [PubMed: 19694452]

Bonet ML, Ribot J, Palou A. Lipid metabolism in mammalian tissues and its control by retinoic acid. Biochim Biophys Acta. 2012; 1821:177–189. [PubMed: 21669299]

Buchner DA, Yazbek SN, Solinas P, Burrage LC, Morgan MG, Hoppel CL, Nadeau JH. Increased mitochondrial oxidative phosphorylation in the liver is associated with obesity and insulin resistance. Obesity (Silver Spring). 2011; 19:917–924. [PubMed: 20885388]

Calvo SE, Mootha VK. The mitochondrial proteome and human disease. Annu Rev Genomics Hum Genet. 2010; 11:25–44. [PubMed: 20690818]

Chen YQ, Zhu J, Lum PY, Yang X, Pinto S, MacNeil DJ, Zhang CS, Lamb J, Edwards S, Sieberts SK, et al. Variations in DNA elucidate molecular networks that cause disease. Nature. 2008; 452:429–435. [PubMed: 18344982]

Deng WJ, Nie S, Dai J, Wu JR, Zeng R. Proteome, Phosphoproteome, and Hydroxyproteome of Liver Mitochondria in Diabetic Rats at Early Pathogenic Stages. Molecular & Cellular Proteomics. 2010; 9:100–116. [PubMed: 19700791]

Fang X, Yu SX, Lu Y, Bast RC Jr. Woodgett JR, Mills GB. Phosphorylation and inactivation of glycogen synthase kinase 3 by protein kinase A. Proc Natl Acad Sci U S A. 2000; 97:11960–11965. [PubMed: 11035810]

Foster LJ, de Hoog CL, Zhang Y, Xie X, Mootha VK, Mann M. A mammalian organelle map by protein correlation profiling. Cell. 2006; 125:187–199. [PubMed: 16615899]

Gnad F, Gunawardena J, Mann M. PHOSIDA 2011: the posttranslational modification database. Nucleic Acids Res. 2011; 39:D253–260. [PubMed: 21081558]

Grimsrud PA, den Os D, Wenger CD, Swaney DL, Schwartz D, Sussman MR, Ane JM, Coon JJ. Large-Scale Phosphoprotein Analysis in Medicago truncatula Roots Provides Insight into in Vivo Kinase Activity in Legumes. Plant Physiol. 2010a; 152:19–28. [PubMed: 19923235]

Grimsrud PA, Swaney DL, Wenger CD, Beauchene NA, Coon JJ. Phosphoproteomics for the masses. ACS Chem Biol. 2010b; 5:105–119. [PubMed: 20047291]

Guan KL, Xiong Y. Regulation of intermediary metabolism by protein acetylation. Trends Biochem Sci. 2011; 36:108–116. [PubMed: 20934340]

Holmstrom MH, Iglesias-Gutierrez E, Zierath JR, Garcia-Roves PM. Tissue-specific control of mitochondrial respiration in obesity-related insulin resistance and diabetes. Am J Physiol Endocrinol Metab. 2012; 302:E731–739. [PubMed: 22252943]

Huttlin EL, Jedrychowski MP, Elias JE, Goswami T, Rad R, Beausoleil SA, Villen J, Haas W, Sowa ME, Gygi SP. A tissue-specific atlas of mouse protein phosphorylation and expression. Cell. 2010; 143:1174–1189. [PubMed: 21183079]

Johnson DT, Harris RA, French S, Blair PV, You J, Bemis KG, Wang M, Balaban RS. Tissue heterogeneity of the mammalian mitochondrial proteome. Am J Physiol Cell Physiol. 2007; 292:C689–697. [PubMed: 16928776]

Keller MP, Choi Y, Wang P, Davis DB, Rabaglia ME, Oler AT, Stapleton DS, Argmann C, Schueler KL, Edwards S, et al. A gene expression network model of type 2 diabetes links cell cycle regulation in islets with diabetes susceptibility. Genome Res. 2008; 18:706–716. [PubMed: 18347327]

Kostiuk MA, Corvi MM, Keller BO, Plummer G, Prescher JA, Hangauer MJ, Bertozzi CR, Rajaiah G, Falck JR, Berthiaume LG. Identification of palmitoylated mitochondrial proteins using a bio-orthogonal azido-palmitate analogue. Faseb J. 2008; 22:721–732. [PubMed: 17971398]

Lea W, Abbas AS, Sprecher H, Vockley J, Schulz H. Long-chain acyl-CoA dehydrogenase is a key enzyme in the mitochondrial beta-oxidation of unsaturated fatty acids. Biochim Biophys Acta. 2000; 1485:121–128. [PubMed: 10832093]

Lee J, Xu Y, Chen Y, Sprung R, Kim SC, Xie S, Zhao Y. Mitochondrial phosphoproteome revealed by an improved IMAC method and MS/MS/MS. Mol Cell Proteomics. 2007; 6:669–676. [PubMed: 17208939]

Lee MV, Topper SE, Hubler SL, Hose J, Wenger CD, Coon JJ, Gasch AP. A dynamic model of proteome changes reveals new roles for transcript alteration in yeast. Mol Syst Biol. 2011; 7:514. [PubMed: 21772262]

McAlister GC, Russell JD, Rumachik NG, Hebert AS, Syka JE, Geer LY, Westphall MS, Pagliarini DJ, Coon JJ. Analysis of the acidic proteome with negative electron-transfer dissociation mass spectrometry. Anal Chem. 2012; 84:2875–2882. [PubMed: 22335612]

Monetti M, Nagaraj N, Sharma K, Mann M. Large-scale phosphosite quantification in tissues by a spike-in SILAC method. Nat Methods. 2011; 8:655–658. [PubMed: 21743459]

Nunnari J, Suomalainen A. Mitochondria: in sickness and in health. Cell. 2012; 148:1145–1159. [PubMed: 22424226]

O'Rourke B, Van Eyk JE, Foster DB. Mitochondrial protein phosphorylation as a regulatory modality: implications for mitochondrial dysfunction in heart failure. Congestive Heart Failure. 2011; 17:269–282. [PubMed: 22103918]

Olsen JV, Macek B, Lange O, Makarov A, Horning S, Mann M. Higher-energy C-trap dissociation for peptide modification analysis. Nat Methods. 2007; 4:709–712. [PubMed: 17721543]

Pagliarini DJ, Calvo SE, Chang B, Sheth SA, Vafai SB, Ong SE, Walford GA, Sugiana C, Boneh A, Chen WK, et al. A mitochondrial protein compendium elucidates complex I disease biology. Cell. 2008; 134:112–123. [PubMed: 18614015]

Pagliarini DJ, Dixon JE. Mitochondrial modulation: reversible phosphorylation takes center stage? Trends Biochem Sci. 2006; 31:26–34. [PubMed: 16337125]

Phanstiel DH, Brumbaugh J, Wenger CD, Tian S, Probasco MD, Bailey DJ, Swaney DL, Tervo MA, Bolin JM, Ruotti V, et al. Proteomic and phosphoproteomic comparison of human ES and iPS cells. Nat Methods. 2011; 8:821–827. [PubMed: 21983960]

Quant PA, Tubbs PK, Brand MD. Glucagon activates mitochondrial 3-hydroxy-3-methylglutaryl-CoA synthase in vivo by decreasing the extent of succinylation of the enzyme. Eur J Biochem. 1990; 187:169–174. [PubMed: 1967579]

Reed WD, Clinkenbeard D, Lane MD. Molecular and catalytic properties of mitochondrial (ketogenic) 3-hydroxy-3-methylglutaryl coenzyme A synthase of liver. J Biol Chem. 1975; 250:3117–3123. [PubMed: 804485]

Ross PL, Huang YN, Marchese JN, Williamson B, Parker K, Hattan S, Khainovski N, Pillai S, Dey S, Daniels S, et al. Multiplexed protein quantitation in Saccharomyces cerevisiae using amine-reactive isobaric tagging reagents. Mol Cell Proteomics. 2004; 3:1154–1169. [PubMed: 15385600]

Schmidt O, Harbauer AB, Rao S, Eyrich B, Zahedi RP, Stojanovski D, Schonfisch B, Guiard B, Sickmann A, Pfanner N, et al. Regulation of mitochondrial protein import by cytosolic kinases. Cell. 2011; 144:227–239. [PubMed: 21215441]

Schwartz D, Gygi SP. An iterative statistical approach to the identification of protein phosphorylation motifs from large-scale data sets. Nat Biotechnol. 2005; 23:1391–1398. [PubMed: 16273072]

Sengupta S, Peterson TR, Laplante M, Oh S, Sabatini DM. mTORC1 controls fasting-induced ketogenesis and its modulation by ageing. Nature. 2010; 468:1100–1104. [PubMed: 21179166]

Shimazu T, Hirschey MD, Hua L, Dittenhafer-Reed KE, Schwer B, Lombard DB, Li Y, Bunkenborg J, Alt FW, Denu JM, et al. SIRT3 deacetylates mitochondrial 3-hydroxy-3-methylglutaryl CoA synthase 2 and regulates ketone body production. Cell metabolism. 2010; 12:654–661. [PubMed: 21109197]

Skaff DA, Miziorko HM. A visible wavelength spectrophotometric assay suitable for high-throughput screening of 3-hydroxy-3-methylglutaryl-CoA synthase. Anal Biochem. 2010; 396:96–102. [PubMed: 19706283]

Syka JE, Coon JJ, Schroeder MJ, Shabanowitz J, Hunt DF. Peptide and protein sequence analysis by electron transfer dissociation mass spectrometry. Proc Natl Acad Sci U S A. 2004; 101:9528–9533. [PubMed: 15210983]

Szendroedi J, Phielix E, Roden M. The role of mitochondria in insulin resistance and type 2 diabetes mellitus. Nat Rev Endocrinol. 2012; 8:92–103. [PubMed: 21912398]

Thompson A, Schafer J, Kuhn K, Kienle S, Schwarz J, Schmidt G, Neumann T, Johnstone R, Mohammed AK, Hamon C. Tandem mass tags: a novel quantification strategy for comparative analysis of complex protein mixtures by MS/MS. Anal Chem. 2003; 75:1895–1904. [PubMed: 12713048]

Villen J, Beausoleil SA, Gerber SA, Gygi SP. Large-scale phosphorylation analysis of mouse liver. Proc Natl Acad Sci U S A. 2007; 104:1488–1493. [PubMed: 17242355]

Wang CY, Stapleton DS, Schueler KL, Rabaglia ME, Oler AT, Keller MP, Kendziorski CM, Broman KW, Yandell BS, Schadt EE, et al. Tsc2, a positional candidate gene underlying a quantitative trait locus for hepatic steatosis. J Lipid Res. 2012a; 53:1493–1501. [PubMed: 22628617]

Wang Y, Li G, Goode J, Paz JC, Ouyang K, Screaton R, Fischer WH, Chen J, Tabas I, Montminy M. Inositol-1,4,5-trisphosphate receptor regulates hepatic gluconeogenesis in fasting and diabetes. Nature. 2012b; 485:128–132. [PubMed: 22495310]

Wenger CD, Lee MV, Hebert AS, McAlister GC, Phanstiel DH, Westphall MS, Coon JJ. Gas-phase purification enables accurate, multiplexed proteome quantification with isobaric tagging. Nat Methods. 2011a; 8:933–935. [PubMed: 21963608]

Wenger CD, Phanstiel DH, Lee MV, Bailey DJ, Coon JJ. COMPASS: a suite of pre- and post-search proteomics software tools for OMSSA. Proteomics. 2011b; 11:1064–1074. [PubMed: 21298793]

Zhao E, Keller MP, Rabaglia ME, Oler AT, Stapleton DS, Schueler KL, Neto EC, Moon JY, Wang P, Wang IM, et al. Obesity and genetics regulate microRNAs in islets, liver, and adipose of diabetic mice. Mamm Genome. 2009; 20:476–485. [PubMed: 19727952]

Zhao X, Leon IR, Bak S, Mogensen M, Wrzesinski K, Hojlund K, Jensen ON. Phosphoproteome analysis of functional mitochondria isolated from resting human muscle reveals extensive phosphorylation of inner membrane protein complexes and enzymes. Mol Cell Proteomics. 2011; 10:M110–000299.

- MS/MS identified 811 phosphorylation sites on 295 mitochondrial proteins in liver
- Over 41% of mitochondrial phospho-isoforms changed across metabolic conditions
- Phosphorylation of serine 456 on Hmgcs2 correlates with ketone body levels in mice
- Hmgcs2 S456 phosphorylation increases enzyme activity and ketogenesis

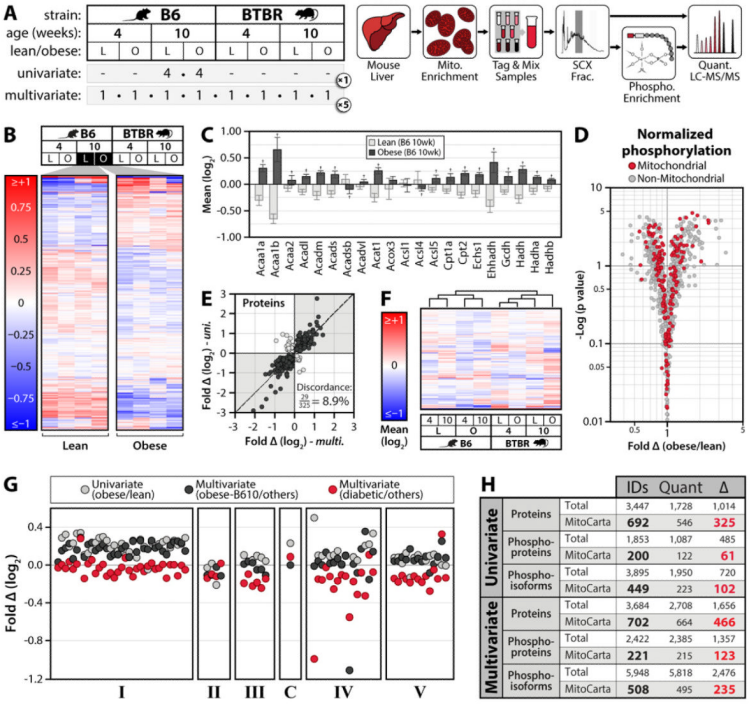

Figure 1. Large-scale, multiplexed proteomic and phosphoproteomic analyses of mouse liver mitochondria

A) We performed our initial analyses in two phases (*left*): a univariate experiment (8 mice, 2 conditions), and a multi-variable experiment (40 mice, all 8 conditions depicted). Our workflow (*right*) involved enriching mitochondria from liver and performing high-resolution quantitative proteomic/phosphoproteomics with 8-plex iTRAQ. B) Unsupervised hierarchical clustering of 4 lean (L) and 4 obese (O) mice (univariate). Values are mean protein abundance, relative to the average of all eight mice, on a $\log_2$ scale from <-1 to >1. C) Abundance of fatty acid oxidation proteins in lean (light grey) and obese (dark grey) mice (univariate), using the same units as *panel B*. Error bars indicate SD and crosses (†) indicate significant differences between lean and obese mice (q<0.1). D) Volcano plot of fold phosphorylation change (normalized to protein abundance) vs. -log (p value) for mitochondrial (red) and non-mitochondrial (grey) phosphosites (univariate). E) Abundance fold-change (obese/lean) for all proteins with significant obesity-dependent alterations (q<0.1) in B6 mice at 10 weeks in both experiments (multivariate on the x-axis and univariate on the y-axis). The percent of measurements in discordance between the two studies (light grey dots) is indicated. F) Unsupervised hierarchical clustering of each condition from the multivariate experiment based on mitochondrial proteins quantified in all five replicates. Values are mean abundance for each condition, relative to all eight conditions, on a $\log_2$ scale from <-1 to >1. G) Abundance fold changes for individual oxidative phosphorylation proteins (each represented by a circle, separated by OxPhos complexes) in the univariate experiment (obese/lean in light grey) and the multivariate experiment (obese 10-week B6 relative to all other conditions in black, obese 10-week BTBR relative to all other conditions in red). See also Table S6. H) Summary of protein and phosphorylation data. IDs, identifications at 1% FDR; Quant, measurements quantified with iTRAQ reporter ions in at least one comparison; (Δ), measurements significantly changing between any condition that was measured (q<0.1). Results are shown for both mitochondrial proteins (MitoCarta) and all proteins identified (Total), in both the univariate and multivariate experiments. See also Figure S1, Table S1-5.

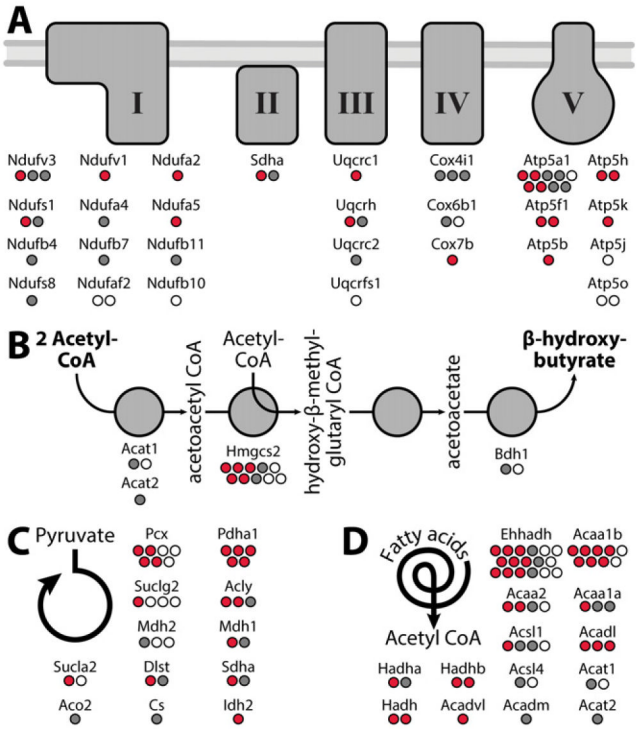

Figure 2. Dynamic phosphorylation of key mitochondrial proteins

A-D) Identification of phosphorylation sites within key mitochondrial pathways: A) oxidative phosphorylation (OxPhos), B) ketone body production, C) the TCA cycle (and related enzymes), D) fatty acid oxidation. Phosphorylation sites exhibiting significant changes ($q<0.1$) are in red; sites that are not changing significantly are in grey; and sites identified, but not quantified are represented as white circles. See also Figure S2.

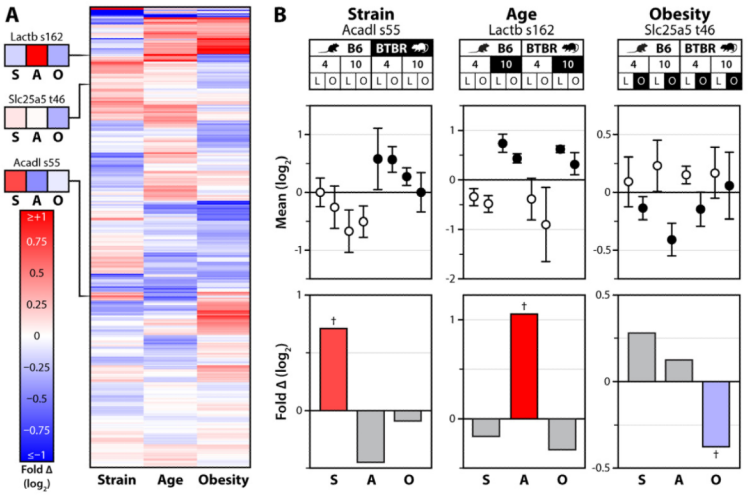

Figure 3. State-specific mitochondrial phosphorylation

A) Heat map showing unsupervised hierarchical clustering of all quantified mitochondrial phosphoisoforms across each single-variable comparison; strain (S), age (A) and obesity (O). Values are fold changes between all mice differing by the indicated variable, on a $\log_2$ scale from <-1 to >1. B) *Top*: 8-plex iTRAQ-based quantification of phosphorylation of Acadl serine 55, Lactb serine 162, and Slc25a5 threonine 46 is shown for each condition (with error bars representing SD from all replicates quantified) relative to the average of all eight conditions. B*ottom:* The same data analyzed with relative abundance reflecting the fold-change ($\log_2$ scale) between all 40 mice of the multivariate experiment separated by one variable at a time (*e.g.*, strain analysis represents all 20 B6 mice vs. all 20 BTBR mice). The colored bars correspond to the comparisons, with the data points highlighted in black on the *top panel* serving as the numerator and those in white as the denominator. Crosses (†) indicate significance at q<0.1.

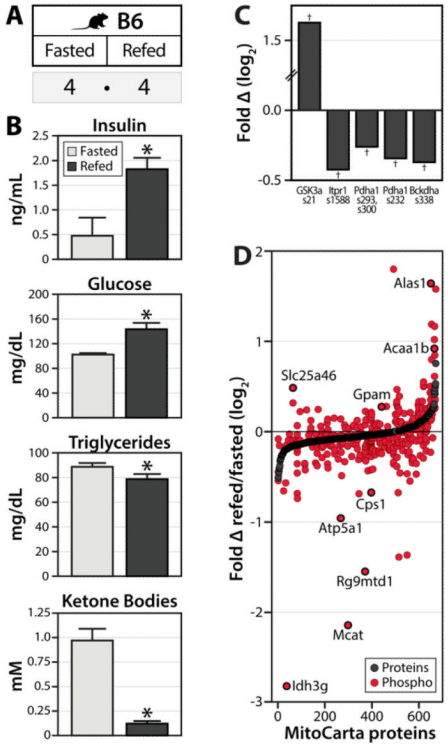

Figure 4. Acute phosphorylation changes across the mitochondrial proteome upon fasting and re-feeding

A) Eight lean B6 mice were fasted overnight (16 hrs), after which half of the animals were allowed to feed *ad libitum* for two hours. Liver mitochondria were isolated and subjected to the same proteomic/phosphoproteomics workflow as described in Figure 1. B) The indicated metabolites were measured from serum, with error bars indicating SEM and asterisks (*) indicating significance at $p<0.05$. C) Phosphorylation fold change (log_2 scale) for selected regulatory site, expressed as refed/fasted with crosses (†) indicating significance at $q<0.1$. D) All mitochondrial proteins (MitoCarta) quantified are ranked on the x-axis by protein abundance fold change (black dots). Relative quantitation of mitochondrial phosphoisoforms (each represented by a single red dot) is plotted at the same position on the x-axis as the corresponding protein measurement. Selected phosphosites of interest are indicated. Note, the few phosphosites for which the corresponding protein was not quantified were assigned a protein fold change of "0" for graphical purposes. See also Table S7.

A

Protein kinase	Sequence preference	MitoCarta phospho-sites	MitoCarta phospho-proteins
CK1	S-X-X-s/t S/T-X-X-X-s	184	111
CAMK2	R-X-X-s/t R-X-X-s/t-V	126	97
GSK3	s-X-X-X-S	111	75
PKA	R-X-s/t R-R/K-X-s/t K-R-X-X-s/t	101	75
CK2	s/t-X-X-E	93	76
CHK1	M/I/L/V-X-R/K-X-X-s/t	45	41
NEK6	L-X-X-s/t	43	37
ERK/MAPK	P-X-s/t-P V-X-s/t-P P-E-s/t-P	35	34
PKD	L/V/I-X-R/K-X-X-s/t	39	36
CDK1	s/t-P-X-K/R s/t-P-K/R	34	30
PLK1	E/D-X-s/t-F/L/I/Y/W/V/M	33	27
PKB/AKT	R-R/S/T-X-s/t-X-S/T R-X-R-X-X-s/t	29	27
CDK2	s/t-P-X-K/R	20	20

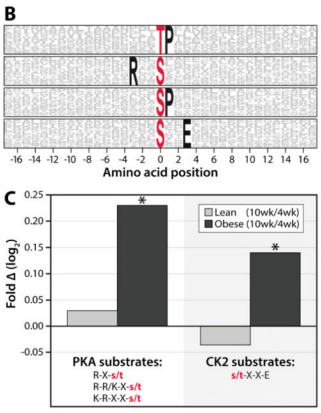

Figure 5. Protein phosphorylation measurements reveal potential kinase-substrate relationships

A) Selected kinases and their substrate consensus sequences from the PHOSIDA database are indicated, with X indicating any amino acid and red lower-case letters indicating the phosphorylated residues. The number of MS/MS-identified mitochondrial phosphorylation sites and phosphoproteins (MitoCarta) that satisfy the sequence preferences for each kinase are listed. B) Motif-X logo indicating amino acid sequence motifs overrepresented around identified phosphorylation sites on MitoCarta proteins. The red letters at position “0” indicate the phosphorylated residue and the probability of an amino acids being present within 17 residues to each side are represented by the height of the respective single-letter symbol. Residues that are “fixed” in the motif (or are always present) span the entire height of the logo and are shown in black (unfixed residues are in grey). C) Relative changes in kinase activity were predicted by averaging phosphosite quantitation for all substrates (mitochondrial and non-mitochondrial) phosphorylated on PKA (*left*) or CK2 (*right*) consensus sites. Values are expressed as fold change (10 week/4 week) on a $\log_2$ scale in both the lean (light grey bars) and obese (black bars) conditions, with asterisks (*) indicating significance at $p<0.05$. See also Figure S3.

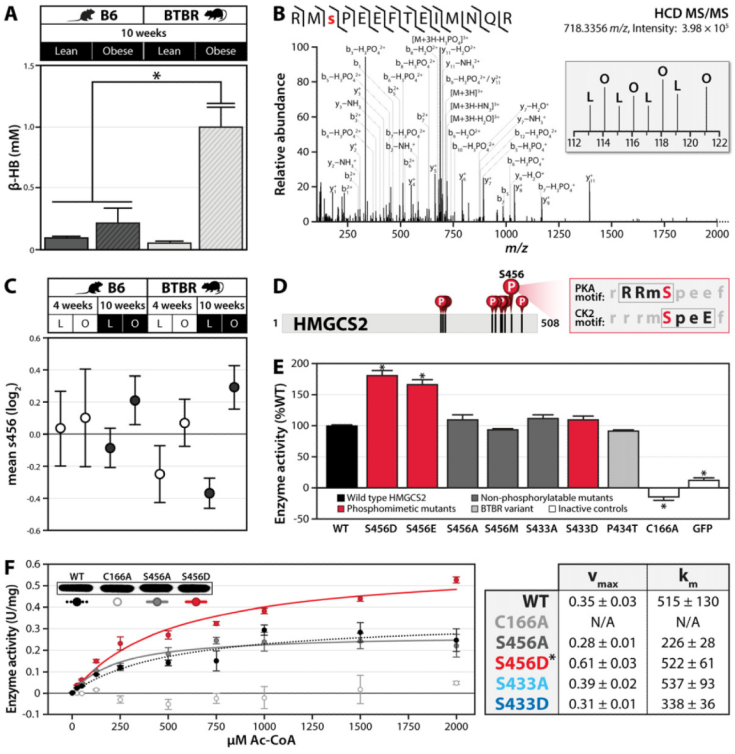

Figure 6. Identification of serine 456 on Hmgcs2 as a candidate regulatory PTM

A) β-hydroxybutyrate (β-HB) levels were measured in serum from lean and obese B6 and BTBR mice at 10 weeks of age. Bars indicate SEM. B) Single scan MS^2 spectrum and manual validation identifying phosphorylation of serine 456 (S456) on mouse Hmgcs2. The *inset* shows iTRAQ reporter ions providing relative quantitation of S456 phosphorylation in lean (L) and obese (O) mice from the univariate study. C) Relative phosphorylation levels on Hmgcs2 S456 in the multivariate experiment. Datapoints indicate condition-specific mean, relative to the average of all eight conditions (log_2 scale), with error bars indicating the SD of all replicates quantified. Note, conditions highlighted in black are the same as those assessed in *panel A*. D) Schematic of Hmgcs2 primary sequence highlighting identified phosphorylated residues, including the PKA and CK2 consensus site at S456. E) Activity of FLAG-tagged wild type (WT) HMGCS2 and the indicated mutants (C166A is catalytically dead control) and GFP, using 1000 μM Ac-CoA as the substrate. Activity is expressed as a percent of WT and error bars indicate SD of triplicate analyses. F) Enzyme activity kinetic curve for FLAG-tagged wild type (WT), S456A, S456D, and C166A HMGCS2. Error bars indicate SD. Kinetic parameters for selected Hmgcs2 variants are shown at the right. Asterisks (*) indicate significance at $p<0.05$. See also Figure S4.

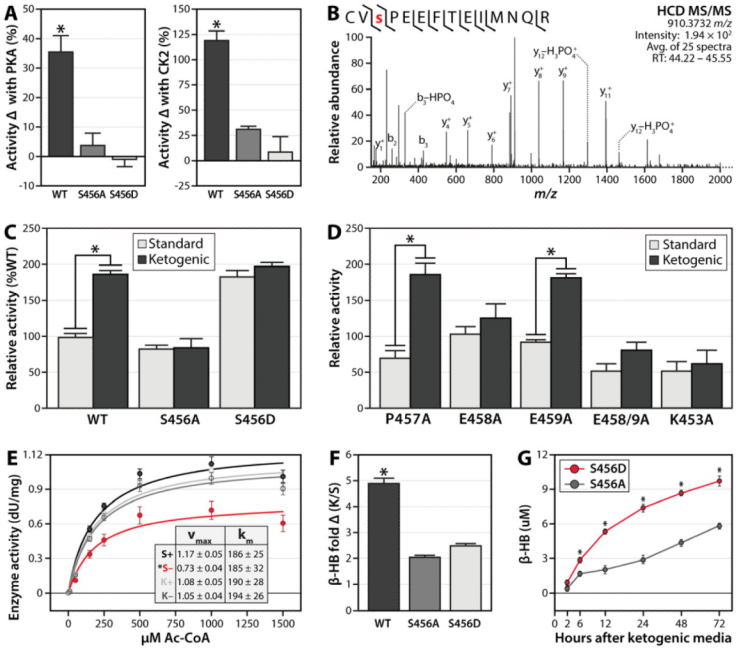

Figure 7. Phosphorylation of serine 456 on HMGCS2 increases enzyme activity and is induced during ketogenesis

A) Percent increase in HMGCS2 activity after performing *in vitro* kinase reactions with either PKA (left) or CK2 (right), error bars indicate SEM. B) Mass spectrum (average of 25 MS^2 scans) identifying phosphorylation of S456 on human HMGCS2 after reaction with PKA seen in *panel A*. C) HMGCS2 enzyme activity at 1000 μM Ac-CoA after immunoprecipitation from HEK293 cells grown in either standard or ketogenic media for 72 hours. Values are normalized to WT in standard media, error bars indicate SEM. D) Activity of HMGCS2 kinase recognition motif mutants, using same assay as in *panel C*. E) Enzyme activity kinetic curve for FLAG-tagged WT HMGCS2 immuoprecitiated from HEK293 cells cultured for 72 hours in either standard (S) or ketogenic (K) media, and subsequently incubated with (+) or without (−) CK2 in an *in vitro* assay. Error bars indicate SD. Kinetic parameters are shown in the *inset*. F) Fold increase in β-hydroxybutyrate (β-HB) levels produced by HEK293 cells expressing HMGCS2 variants upon culturing in ketogenic (K) media for 72 hours, relative to standard (S) media. G) β-hydroxybutyrate (β-HB) levels in S456A (grey) or S456D (red) mutant HMGCS2-transfected HEK293 cells over a timecourse of culturing in ketogenic media. Asterisks (*) indicate significance at $p<0.05$. See also Figure S5.